A&A 393, 273–283 (2002)
DOI: 10.1051/0004-6361:20020996

Astronomy & Astrophysics

Small scale structure in circumstellar envelopes and the origin of globules in planetary nebulae⋆

P. J. Huggins[1] and N. Mauron[2]

[1] Physics Department, New York University, 4 Washington Place, New York NY 10003, USA
[2] Groupe d'Astrophysique, CNRS & Université de Montpellier, Case 072, Place Bataillon, 34095 Montpellier Cedex 05, France

Received 17 June 2002 / Accepted 21 June 2002

Abstract. We analyze the small scale structure in the circumstellar envelopes of NGC 7027 and IRC+10216, using high resolution optical images in dust scattered light. We use the observations to test the proposal that globules in planetary nebulae, typified by globules in the Helix nebula, originate in high density contrast proto-globules in the atmosphere of the progenitor AGB star and are carried out in the circumstellar wind (Dyson et al. 1989). We find no evidence for the presence of proto-globules in the extended envelopes of NGC 7027 and IRC+10216 with the expected sizes and masses $\gtrsim 10^{-5}$ $M_{\odot}$ which are needed to produce globules like those in the Helix nebula. We do find azimuthal structure in the envelopes on size scales of $l \gtrsim 0.1d$ where d is the radial distance, consistent with the smoothing out of small scale structure by thermal motions in the wind acceleration region. Unless globules require special conditions not found in NGC 7027 or IRC+10216, which are among the most likely precursors of Helix-like nebulae, our results argue against their origin in the atmosphere of the central star. We suggest alternative scenarios for globule formation, including the fragmentation of the neutral circumstellar gas at the transition phase by directed outflows or jets.

Key words. stars: AGB and post-AGB – stars: mass-loss – stars: individual: IRC +10216 – stars: circumstellar matter – planetary nebulae: general – planetary nebulae: individual: NGC 7027

1. Introduction

High resolution optical observations of planetary nebulae (PNe) have produced striking images of small-scale structure within and around the periphery of the ionized gas. The best known example of this micro-structure is the remarkable array of cometary globules seen in the Helix nebula (NGC 7293). The heads of Helix globules are ∼1″–2″ in size, with photo-ionized surfaces facing the central star, and radially extended tails pointing in the opposite direction (e.g., Meaburn et al. 1992; O'Dell & Handron 1996). They consist of dense knots of cool, molecular gas and this accounts for their relative longevity (Huggins et al. 1992, 2002; Dyson et al. 1989). The Helix is the best studied PN with globules because it is one of the nearest PNe and can be observed with the highest spatial resolution. There is, however, good evidence for similar globules in other, more distant PNe, e.g., in NGC 6720 (O'Dell et al. 2002), and they are probably a general characteristic of PNe with envelopes of neutral gas (Huggins et al. 1996).

Two extreme classes of model have been proposed to explain the origin of globules in PNe. In the first, due to Dyson et al. (1989), the globules are formed as the result of an instability in the atmosphere of the progenitor, asymptotic giant branch (AGB) star, and are then carried out as coherent objects to their observed positions in the general wind flow. In the second class of model (e.g., Capriotti 1973), the globules are formed far from the central star, from an initially homogeneous envelope, as the result of an instability at or near the ionization front of the nebula.

In this paper we examine the question of globule formation by studying the small scale structure in two archetypical circumstellar envelopes, IRC+10216 and NGC 7027. We directly test the proposal that globules are formed by the progenitor AGB star and are carried out to their observed positions, by searching for the expected proto-globules in the extended envelopes. We find no evidence for such structures with the relevant mass and size scales. We conclude that the globules are formed at a later stage, and comment on the possible role of multiple shells and multiple jets in the formation process.

2. The circumstellar envelopes

2.1. General properties

The archetypes IRC+10216 and NGC 7027 that we examine provide the best opportunities to study small scale structure

Send offprint requests to: P. J. Huggins,
e-mail: patrick.huggins@nyu.edu

⋆ Based on de-archived observations made with the NASA/ESA *Hubble Space Telescope*, operated by AURA Inc. under NASA contract NAS5-26555, and on observations made with the VLT in Paranal (Chile), operated by ESO (program 64L–0204A).

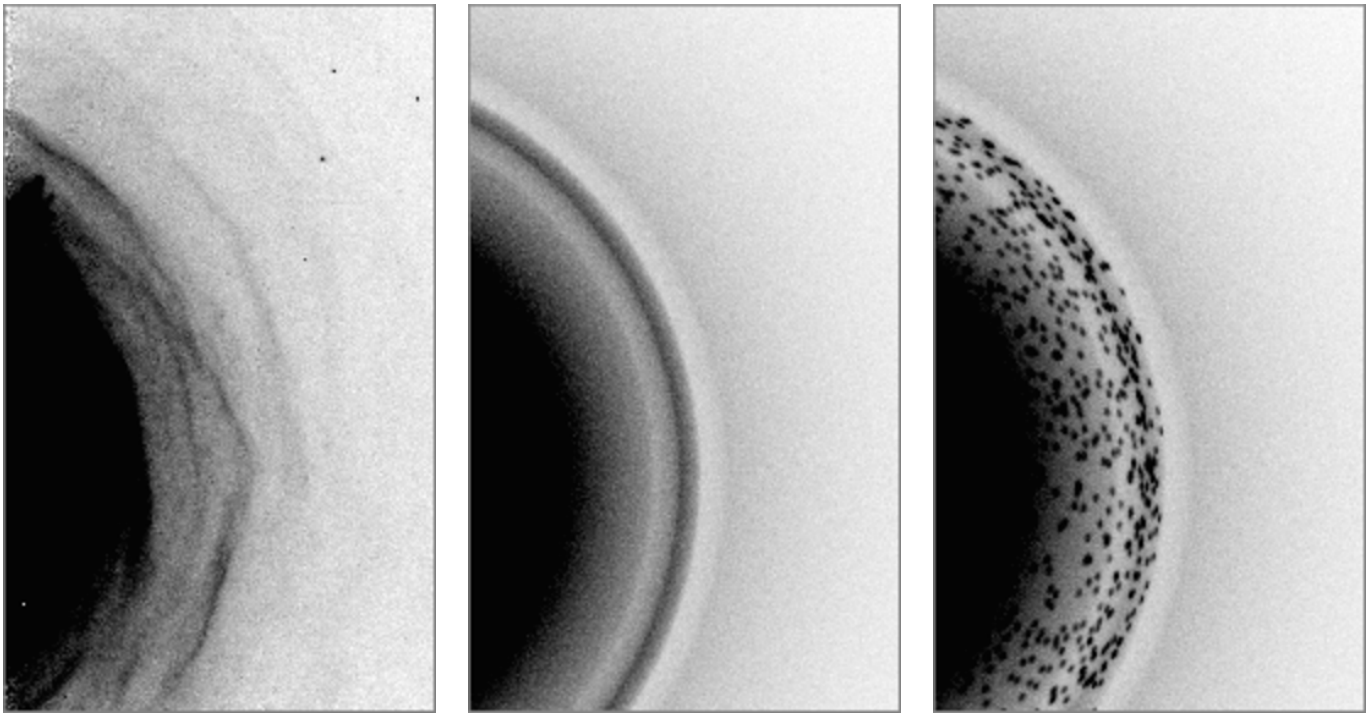

Fig. 1. The circumstellar envelope of NGC 7027 in scattered light. *Left*: HST image in Hα. it Center: simulation a with a smooth shell profile. *Right*: simulation c with proto-globules of mass 3×10^{-5} $M_{\odot}$; see Table 2 for details. The fields are $17\farcs7 \times 29\farcs0$ with $0\farcs1$ pixels.

Table 1. Properties of the envelopes.

Name	D (pc)	V (km s^{-1})	$\dot{M}$ ($M_{\odot}$ yr^{-1})
IRC+10216	120	14	1.6×10^{-5}
NGC 7027	880	15	1.6×10^{-4}

in extended circumstellar envelopes at high spatial resolution. IRC+10216 is the nearest, carbon-rich AGB star with a high mass-loss rate, and NGC 7027 is a young PN, still surrounded by the extended, neutral envelope ejected on the AGB. These objects represent different stages in the AGB–PN transition, and are among the most likely progenitors of evolved PNe like the Helix nebula which still retain a substantial envelope of neutral gas (Huggins et al. 1996). Table 1 lists some properties of the envelopes for later discussion, the distance D, the expansion velocity V, and the mass loss rate ($\dot{M}$) measured in CO (adapted from Loup et al. 1993; Masson 1989; Huggins et al. 1988; Jaminet et al. 1991).

We study the small scale structure of these circumstellar envelopes using images in dust-scattered optical light. It is assumed that the dust traces the mass in the envelopes although the exact degree of dust-gas coupling is an open question. For our purposes, however, we note that the dust and gas in IRC+10216 show the same structure to the extent that it can currently be determined (Mauron & Huggins 2000), and in the Helix globules themselves, the dust-to-gas ratio is not anomalous (Meaburn et al. 1992; Huggins et al. 1992), i.e., there has been no major separation of dust and gas in the material from which the globules formed.

2.2. Observations in scattered light

2.2.1. NGC 7027

The observations of NGC 7027 that we consider consist of two 1000 s exposures made through the narrow Hα filter (F656N) with the Wide Field Camera (WFPC2) on board the Hubble Space Telescope. The data have been retrieved from the telescope archives (Project No. 6280, PI Westphal) after processing by the WFPC2 pipeline, which includes bias subtraction, flat-fielding, and correction for cosmic ray defects. The image that we use (Fig. 1, left) has been extracted from the one of four WFPC2 panels that provides good coverage of the scattered nebular light in the extended circumstellar envelope and is least affected by defects due to saturation at the center of the main nebula. The complete nebular system is shown by Bond (2000), and the panel we use is at the lower right of his Fig. 4.

The pixel size of the image in Fig. 1 is $0\farcs1$. The image is saturated at a level of 4000 ADU near the center of the left hand side, and the intensity falls rapidly across the envelope to a level near the sky background of ~2 ADU at the right.

The intensity of the extended Hα outside the main nebula, varies as $\sim r^{-3}$–r^{-4}, consistent with optically thin scattering of nebula light by the dust envelope, as first discussed by Atherton et al. (1979); see also Latter et al. (2000). Scattering by the envelope has been directly confirmed by high levels of polarization seen in [O III] and Hα outside the main nebula by Walsh & Clegg (1994). The radial structure in the envelope has been discussed by Bond (2000) and Kwok et al. (2001).

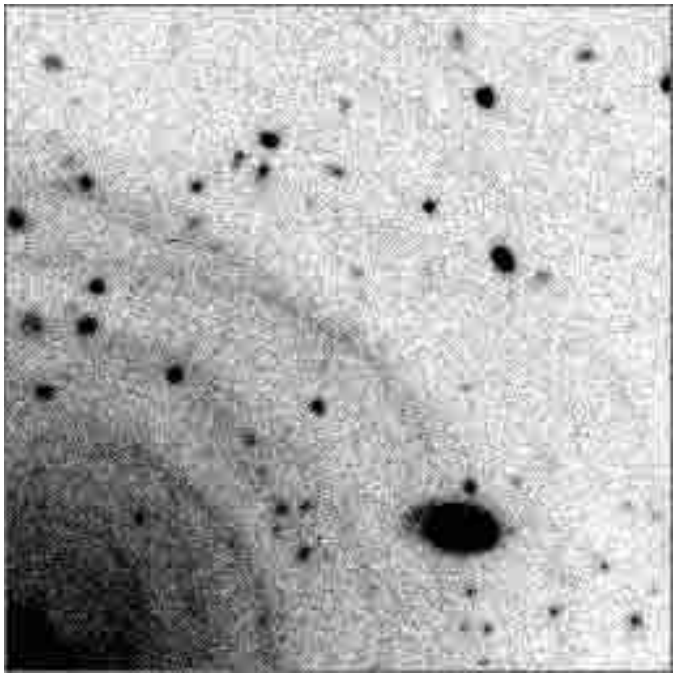

Fig. 2. VLT V-band image of the circumstellar envelope of IRC+10216 in scattered light. The field is $51\farcs2 \times 51\farcs2$ and the star is located at the lower left corner.

2.2.2. IRC+10216

The observations of IRC+10216 that we use consist of deep V band imaging of the circumstellar envelope obtained with the VLT (for details see de Laverny 2002). The region of interest to the north west of the central star where the envelope is most clearly seen is shown in Fig. 2. The pixel size is $0\farcs2$, the seeing is $0\farcs64$ (FWHM), and the count level decreases from 2720 ± 15 ($1\,\sigma$) ADU in the bottom left (near the central star), to 2615 ± 15 ADU in the top right. The discrete background consists of numerous, faint galaxies.

The envelope of IRC+10216 is seen in the image in dust-scattered, ambient, Galactic light (although very close to the center the light from the star is seen). The radial variation is consistent with optically thin scattering, except within $\sim 10''$ of the center where the envelope becomes optically thick and the intensity reaches a roughly constant, plateau level. Limb-brightened multiple shells are clearly seen in the envelope, and have been described in detail by Mauron & Huggins (1999, 2000).

3. Proto-globules

We focus our analysis of the micro-structure in the circumstellar envelopes by first outlining what might be expected according to the model of Dyson et al. (1989) in which globules originate close to the progenitor AGB star. In this model, the globules initially form as high density contrast, low temperature (10–25 K), neutral condensations in the extended atmosphere of the star as the result of a thermal or possibly a magnetic instability (Hartquist & Dyson 1997). These proto-globules then move out as coherent objects in the wind flow, and are finally seen as high density-contrast, neutral globules when they have been overtaken by the ionized nebula.

If this proposal is correct, the proto-globules must be present in the extended, neutral, circumstellar envelopes, and they should in principle be detectable at this evolutionary phase. The angular resolution of millimeter molecular line observations is currently too low to search for the proto-globules, but they are potentially observable in the high resolution optical images in dust scattered light described above.

Key parameters in a search for the proto-globules are their mass ($M_{\rm pg}$), radius ($r_{\rm pg}$), and their scattering properties. In the analysis that follows we adopt a representative, standard value for the mass of a proto-globule of $3 \times 10^{-5}\ M_\odot$, based on observations of the Helix globules. The adopted value is a factor of $\sim$2 larger than lower limits on the masses of globules detected in CO by Huggins et al. (1992) for an assumed distance to the Helix of 200 pc, and so makes some allowance for atomic gas in the globules, as well as possible ablation during their envelopment by the ionized nebula. This standard mass is well below the mass range for proto-globules discussed by Dyson et al. (1989) based on survival considerations (10^{-4}–$10^{-3}\ M_\odot$), but these higher mass structures would be correspondingly easier to detect.

Following Dyson et al. (1989), the proto-globules are assumed to form with a characteristic size $l_{\rm o}$ close to the star and then to expand with the local sound speed $c_{\rm o}$ while being carried out in the wind with a velocity V (which is assumed to be comparable with the expansion velocity of the envelope). At time t, the radius of the proto-globule is given by $r_{\rm pg} = l_{\rm o} + c_{\rm o} t$, and the radial distance from the star (d) is given by $d \sim Vt$. Thus for large t, $r_{\rm pg}/d = c_{\rm o}/V$. Using representative average values of $c_{\rm o} = 0.2$ km s^{-1} (H_2 gas at 10 K) and $V = 15$ km s^{-1}, $r_{\rm pg} = 0.013\,d$ gives an estimate of the proto-globule size as it moves away from the star. The globule will also be somewhat flattened (Dyson et al. 1989) and we adopt a nominal flattening by a factor of 4 in the radial direction.

The simple description given here means that the proto-globules subtend a roughly constant angle of $\sim 1\fdg5$ at the central star. Currently, the globules in the ionized gas of the Helix nebula subtend a somewhat smaller angle of $\sim 0\fdg5$ at the star, but this is quite consistent with the general scenario because they are expected to have been somewhat compressed by the increased pressure that occurred when they were overtaken by the ionized nebula.

The final quantity needed to determine the observability of the globules is a relation between their scattering properties and their mass or column density. In the general case this would require a detailed knowledge of the grains, their opacity, and the dust-to-gas ratio. In practice, we estimate the scattered intensity of a model globule with a specified column density by comparing it with the envelope along the same line of sight (for which the density and column density are known from the mass loss rate) and then by scaling to the observed intensity of the envelope. In this way the most important uncertainties essentially cancel out. In both cases considered below, the envelopes can be considered to be reasonably optically thin in the directions considered. For the opacity of the proto-globules, we use the Helix globules as a guide. These have extinction

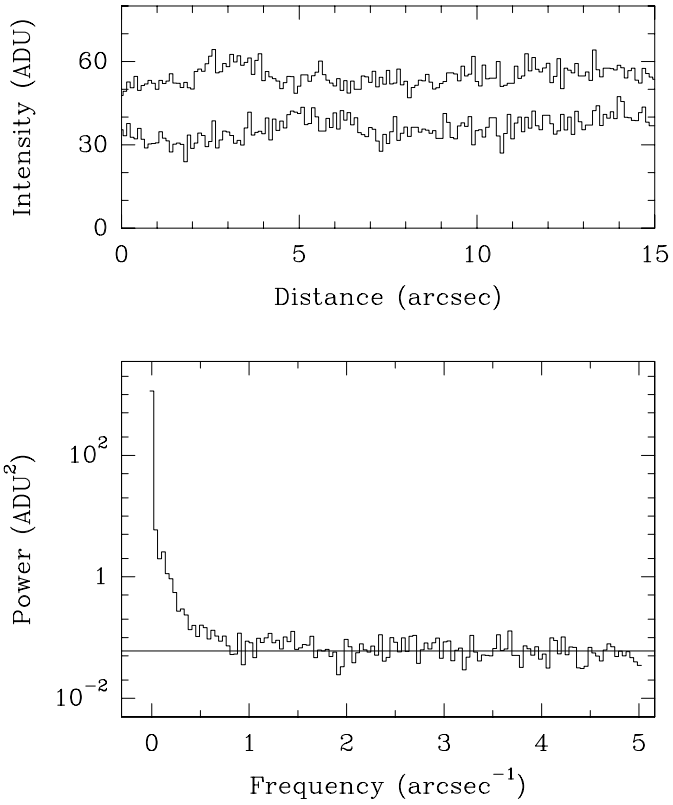

Fig. 3. Characteristics of the scattered light image of NGC 7027. *Top*: representative intensity strips in azimuth at radii of 16.″2 and 18.″2; the latter has been shifted vertically for clarity. *Bottom*: average power spectrum of 10 intensity strips 256 × 0.″1 in azimuth at radii 16.″2–18.″2.

optical depths of ∼0.5 through the center (Meaburn et al. 1992; O'Dell & Handron 1996), and for our proto-globules we scale this according to the globule size and mass.

4. NGC 7027

4.1. Overview

The image of NGC 7027 in Fig. 1 shows the prominent radial structure of the envelope, but otherwise appears relatively smooth on small scales, with no obvious evidence for discrete proto-globules. In order to characterize the smoothness we have extracted intensity strips in azimuth from a sector of the image in Fig. 1 between radii 16.″2–18.″2 with 0.″1 spacing, using nearest pixel intensities to preserve the noise characteristics of the image. The mean intensity of the sector is 33.8 ADU, the rms noise level is 4.3 ADU and the noise contribution to this from photon statistics is 2.4 ADU. The upper panel of Fig. 3 shows representative intensity strips from the sector and the lower panel shows the average power spectrum of ten strips. The frequency of the upper end of the power spectrum (5 arcsec^{-1}) is set by the Nyquist frequency and corresponds to variations on a size scale of 0.″2. The peak of the power spectrum at zero frequency corresponds to the mean intensity squared.

Except for the lowest frequencies, the power spectrum is seen to be essentially flat. A flat spectrum is indicative of white noise, and the observed level (indicated by the horizontal line in the figure) corresponds to an rms which is 14% above the level expected from photon statistics alone. Given that there are other sources of noise in addition to the photon statistics, e.g., slightly different radial gradients across the strips, there is no evidence for an important contribution to the noise from small scale, discrete structures. On the other hand, there is significant power at frequencies $\lesssim$0.5 arcsec^{-1}, i.e., on angular size scales of $\gtrsim$0.12 rd or 7° as seen from the central star. These variations account for the major contribution to the observed variance, and are partly due to the non circularity of the prominent shells, and partly to intrinsic variations in azimuth.

The statistics, therefore, provide clear evidence for large scale structure in the envelope, but no evidence for small, discrete structures above the level of the photon noise.

4.2. Simulations

In order to test for the presence of specific small scale structures of the type outlined in Sect. 3, we have carried out simulations with different assumptions concerning the mass, size, and number of possible proto-globules that the envelope might contain. For each case, we generate a synthetic image in scattered light for comparison with the observations, focusing on the region discussed above and shown in Fig. 1.

For the envelope we use a simple, spherically symmetric model with a constant, average mass-loss rate (Table 1), but within a radius range of 17″ ± 1.″5 we compress the material into a shell of thickness 0.″85 (a compression by a factor of 3.5) to roughly reproduce the structure observed in this region. This is in fact not an essential feature of our analysis, but it facilitates comparison with the observations. A certain mass fraction (f) of the shell is assumed to form $N_{\rm pg}$ discrete proto-globules, of mass $M_{\rm pg}$ and radius $r_{\rm pg}$, and the remainder (1–f) is smoothly distributed in the shell. The proto-globules are flattened in the radial direction by a factor of 4, and are randomly distributed within the shell without overlapping.

From the discussion of section 3, the diameter of a standard proto-globule at a distance of 17″ (2.2×10^{17} cm) from the star is 0.″45 (6.0×10^{15} cm), and it would therefore be resolved by the observations. The optical depth through the center of the globule would be ∼0.2 along the short axis and ∼0.8 along the long axis. For simplicity, we take this to be optically thin for the model calculations, bearing in mind that we will overestimate the scattered intensity of a globule seen close to edge-on by ∼50%. The illumination is from the center, and we assume the scattering is isotropic, but the effects of a more realistic phase function essentially cancel out since we compare the emission from the proto-globules with the average emission from the envelope in the same region. A synthetic image of scattered light from the envelope is calculated over a grid of pixels of size 0.″025 and is convolved with the HST point spread function at the wavelength of Hα. The image is then resampled at the resolution of the observations (0.″1), scaled to the intensity level of the sector, and photon noise is added for comparison with the actual data.

Details of the simulations are listed in Table 2. In addition to the parameters already discussed, we also list the globule

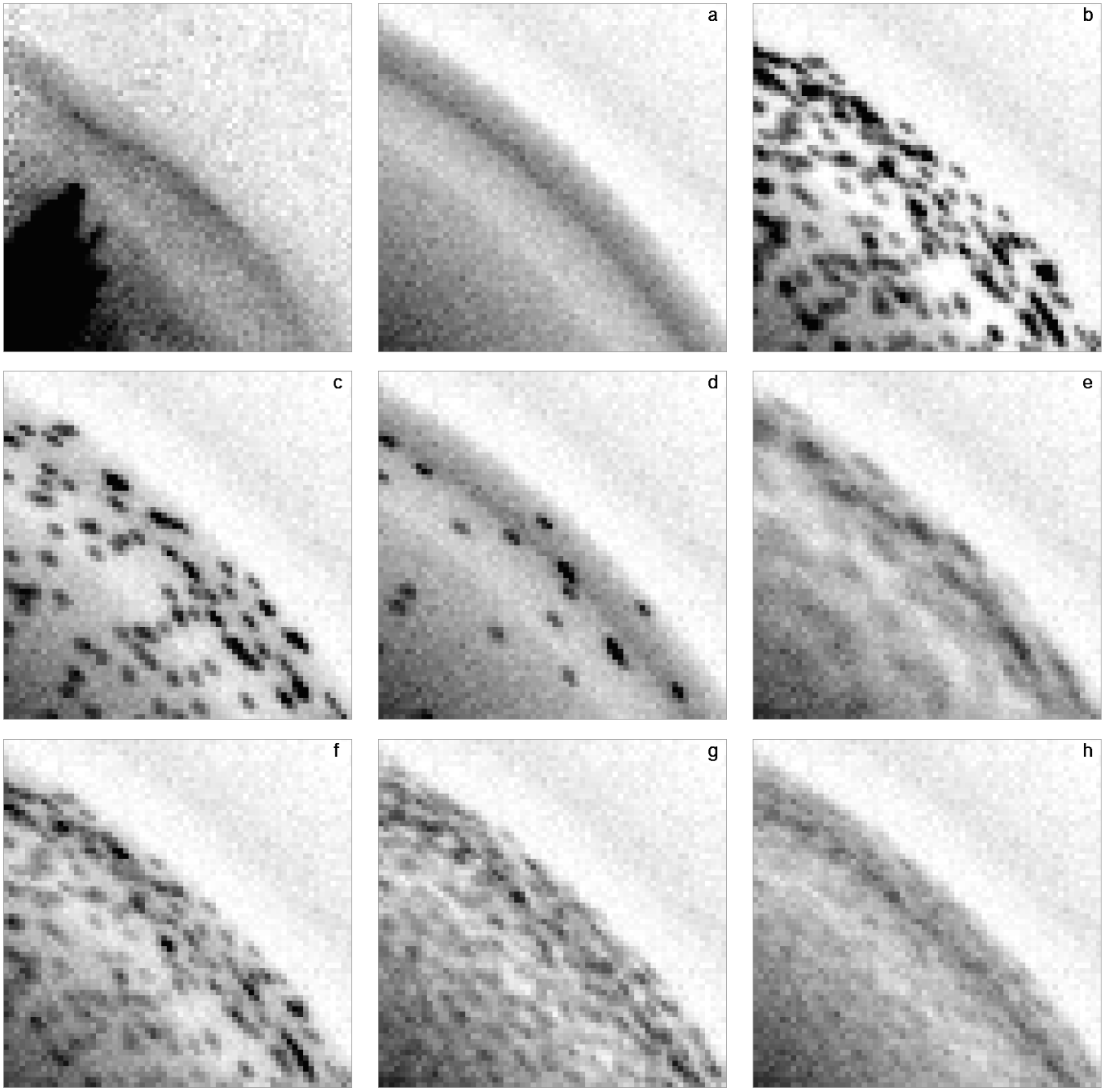

Fig. 4. Close-up image and simulations of the envelope of NGC 7027. *Left to right, top to bottom:* observed image, and simulations **a)**–**h)** in sequence. See Table 2 for details. The fields are $6\farcs4 \times 6\farcs4$ with $0\farcs1$ pixels.

density relative to a completely smoothed out, constant mass-loss envelope ($\rho_{\rm pg}/\rho_{\rm env}$), and relative to the actual ambient density in the shell ($\rho_{\rm pg}/\rho_{\rm sh}$).

4.3. Results for NGC 7027

The results of the simulations are compared with the observations in close-up images in Fig. 4 and intensity strips in azimuth in Fig. 5. Wider field images of simulations a and c are also shown in the center and right hand panels of Fig. 1.

Inspection of the figures shows that the simulation most resembling the observed image is model a (Fig. 4 top, center), which consists of a smooth shell with no proto-globules at all. The main difference between the simulated and observed images is the presence in the latter of large scale ($\gtrsim 2''$) variations which were already noted in Sect. 4.1. These variations are not caused by proto-globules, but are the result of moderate azimuthal variations (with column density changes of ~50%) and deviations of the ring structure from spherical symmetry.

Envelopes containing standard globules (with masses of $3 \times 10^{-5}\ M_\odot$) of the type hypothesized by Dyson et al. (1989)

Table 2. Simulations of NGC 7027.

Model	M_{pg} ($M_\odot$)	N_{pg}	ρ_{pg}/ρ_{env}	ρ_{pg}/ρ_{sh}	f	Comments
a	...	0	...	...	0	smooth shell, no globules
b	3.0×10^{-5}	4450	202	∞	1.0	standard globules
c	3.0×10^{-5}	2225	202	115	0.5	standard globules
d	3.0×10^{-5}	445	202	64	0.1	standard globules
e	1.9×10^{-5}	3465	17	9	0.5	$M_{pg} = M_{st}/1.6$ $r_{pg} = 2\,r_{st}$
f	1.5×10^{-5}	4450	101	57	0.5	$M_{pg} = M_{st}/2$
g	6.6×10^{-6}	20 227	44	∞	1.0	$M_{pg} = M_{st}/4.5$
h	3.3×10^{-6}	20 227	22	13	0.5	$M_{pg} = M_{st}/9$

are shown in simulations b–d for different mass fractions of the shell in globules. In simulation b, the whole shell is in the form of globules, which are closely packed and overlap along many lines of sight in the image, resulting in a strong, mottled pattern. Simulation c is an intermediate case, and in simulation d only 10% of the shell mass is in globules which overlap only rarely in the image. In each case the globules are clearly seen with a high signal-to-noise ratio, and although we may have overestimated the intensity of those seen edge-on by ∼50%, we can rule out this type of envelope structure. Also, if we have significantly underestimated the opacity of the globules so that they are optically thick in the radial direction, those on the near side of the envelope would be easily seen in absorption against the shell background, but there is no evidence for this in the observations.

The visibility of individual globules (as in simulation *d*) in the optically thin scattering limit can be obtained in an analytic approximation when the globule is spatially resolved. If we express the peak intensity of the scattered light from the proto-globule relative to the background envelope (assumed to have a smooth, constant mass loss rate) as I_{pg}/I_{env}, then it can be shown for an ellipsoidal globule (flattened by a factor of 4) seen edge-on in the plane of the sky at a distance d from the star, that $I_{pg}/I_{env} = (48 M_{pg} V d)/(\pi \dot{M} r_{pg}^2)$. For a standard globule in NGC 7027 at an offset of 17″ and the envelope parameters given in Table 1, $I_{pg}/I_{env} \sim 3$. In simulation d this estimate is modified somewhat by the presence of the shell and by the fact that the globule seen edge-on is only partly resolved, so the ratio is closer to ∼1. Nevertheless, if the envelope is detected with a good signal-to-noise ratio, the globule is easily seen.

Simulations e–h explore variations of the proto-globule parameters. The proto-globules are unlikely to be significantly smaller than the standard case because the average dispersion velocity that we have adopted is likely close to the minimum it could be, and the proto-globules are unlikely to be pressure confined in the tangential direction. They could be somewhat larger, and model e is for low density contrast globules, with the diameter increased by a factor of 2 and the mass reduced by a factor of 1.6, so the density contrast is lower by a factor of ∼12; these are also well seen in the simulated image. Significantly larger, very low density structures could be present in the envelope and remain unseen, but such structures would not be identified with the coherent proto-globules under discussion.

The observability of individual proto-globules of lower mass can be assessed by scaling the results of simulation d or using the analytic result given above. For the S/N ratio of the current observations, we can rule out globules with the same size as standard globules but with masses lower by factors of ∼5–10, i.e., $M_{pg} \lesssim 3\text{–}6 \times 10^{-6}$. Simulations f–h consider large numbers of these lower mass globules, and each simulated image is noticeably more granular than the observations, with simulation h being close to a limiting case. The bottom line of the analysis is that the envelope of NGC 7027 is relatively smooth and does not include high density contrast proto-globules.

5. IRC+10216

5.1. Overview and simulations

Our analysis of IRC+10216 follows that of NGC 7027, but with some important differences: the illumination is external, standard proto-globules (if present) are optically thick, and the characteristics of the observations are different. The sky background of Fig. 2 is much stronger than for NGC 7027 and is the dominant source of noise, with the S/N per pixel lower by a factor of ∼3. There are also some discrete features in the image, but we believe that essentially all are background galaxies or stars. The larger and brighter objects are brighter than the plateau region (see below) and are immediately ruled out as scattering centers in the envelope, and the more numerous, fainter features show no statistical variation in number per unit area, or size, versus distance from the center of the envelope, which indicates that most or all are background objects

We focus on a region ∼34″ to the north west of the central star roughly in the center of the field of Fig. 2 where the envelope is well seen. The shell intensity in this region is ∼35 ADU above the background, and is a factor of ∼3 below the plateau level seen near the center of the envelope, which corresponds to the scattered intensity of an optically thick envelope (see Mauron & Huggins 1999, 2000). We have extracted 10 circular strips covering the shell in this quadrant and find that the average rms level (with the bright, discrete features masked) is 16.6 ADU. This is only marginally above the sky background (∼15 ADU), so there is no evidence for a significant contribution from small scale structure in the envelope. This is confirmed by constructing the average power spectrum of the

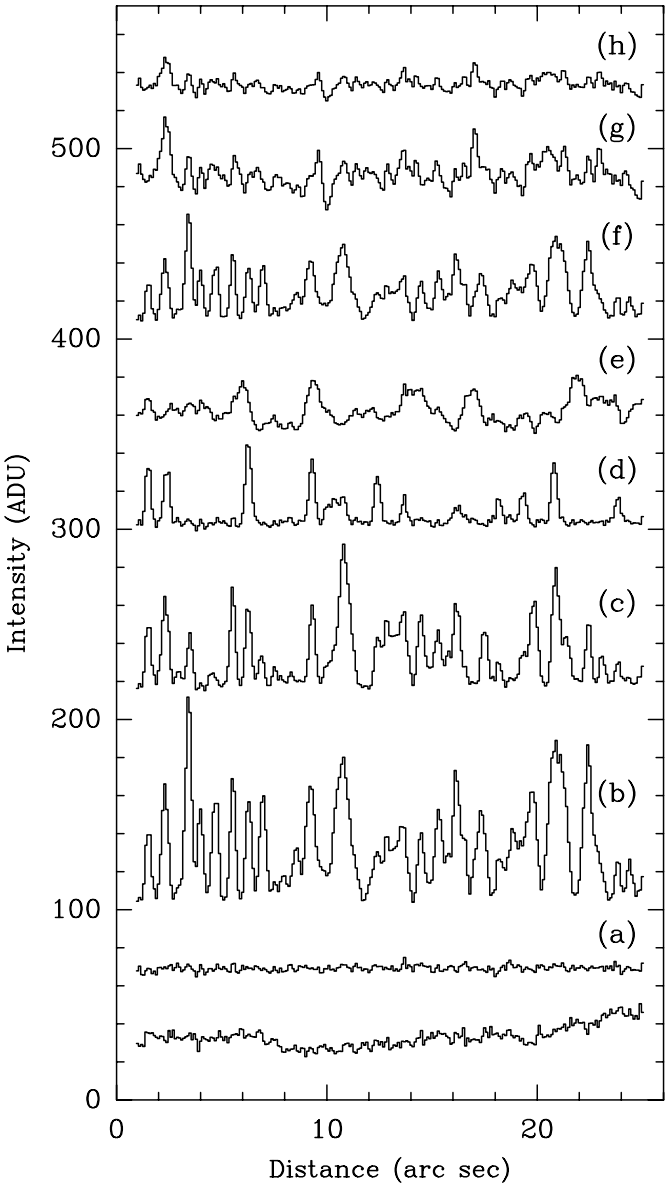

Fig. 5. Intensity strips of the envelope of NGC 7027 (bottom) and simulations a–h shown in Fig. 4. The strips are interpolated at 0.″1 spacing in azimuth at a radius of 17″, and are offset along the vertical axis for clarity.

strips, which is similar to that of NGC 7027 shown in Fig. 3. Most of the spectrum is fairly flat, at the level expected from the sky background, but there is significant power at low frequencies $\lesssim$0.2 arcsec^{-1} which corresponds to length scales of $\gtrsim$5″, i.e., $\gtrsim$0.14 rd as seen from the central star. In fact, the fairly long-range azimuthal coherence of the shells is evident from visual inspection of Fig. 2.

At the distance of IRC+10216 (Table 1), an offset of 34″ corresponds to 6.1×10^{16} cm, so the observed material is closer to the star than in the case of NGC 7027 or the Helix nebula. The hypothesized standard proto-globules will therefore be smaller, with a diameter of $\sim1.6\times10^{15}$ cm, but the angular size (0.″9) is not too unfavorable for ground based observations because IRC+10216 is relatively nearby. From the scaling given in Sect. 3 we expect standard globules to be optically thick, with $\tau\sim12$ for the long axis and $\sim$3 for the short axis, and because of the external illumination they will shine with roughly the same intensity as the optically thick plateau region near the center of the envelope.

To investigate the presence of such structures, we have carried out simulations as before, assuming a shell whose thickness (2.″4) and compression (2.5) roughly reproduce the observed shell structure seen in the center of Fig. 2. For a range of proto-globule masses and sizes, and different mass fractions of the shell, we compute the intensity on a grid of pixels of size 0.″05, approximating the optically thick lines of sight by clipping the pixel values at the observed level of the optically thick plateau. We then convolve with the point spread function, group the pixels 4×4, scale to the envelope signal, and add the sky background and the noise at the level seen in the observations. Because of the limited S/N of the observations, we have also smoothed both the observations and the simulations with a Gaussian of 0.″33 (*FWHM*). Details of the simulations are given in Table 3.

5.2. Results for IRC+10216

The results are compared with the observations in close-up images in Fig. 6. We note that the bright, discrete feature at the bottom of the observed image (Fig. 6, top left) is brighter than the plateau and is therefore a foreground or background object. The fainter discrete feature at the top of the image is also unrelated to the envelope with a high probability by the arguments given in the previous section. We ignore both features in the discussion.

Model a of the envelope which contains only a smooth shell and no globules at all (Fig. 6, top center) matches the observations within the noise. Models b–d are for standard globules in the shell. They are fewer in number than in the case of NGC 7027 because of the lower mass-loss rate in IRC+10216. If 100% or 50% of the shell is in proto-globules (models b and c), they are well seen in the simulated images. However, with only 10% in globules (model d), only 1 or 2 fall within the 12.″8 field, and they cannot readily be seen against the gradient of the shell background. Does this mean that standard proto-globules would go undetected in the envelope if they constitute $\lesssim$10% of the mass? The answer to this is no. The globules are optically thick and are, in fact, bright relative to the shell, but appear weak in simulations b–d because they are not well resolved when seen close to edge-on. However, standard proto-globules a little farther out in the envelope would be larger, and would be seen more face-on along the line of sight in the figure. An example is shown in model e, where a few globules at a radius 50% larger than the shell (51″) appear along the line of sight: they are easily seen against the full shell. Standard globules farther out would be even more prominent.

Simulations f–h explore variations of the proto-globule parameters. Model f is for lower density-contrast globules with the diameter increased by a factor of 2. These are now well resolved, even when close to edge-on, and are easily seen. Models g and h are for larger numbers of proto-globules with less mass: simulation g is noticeably more granular than the

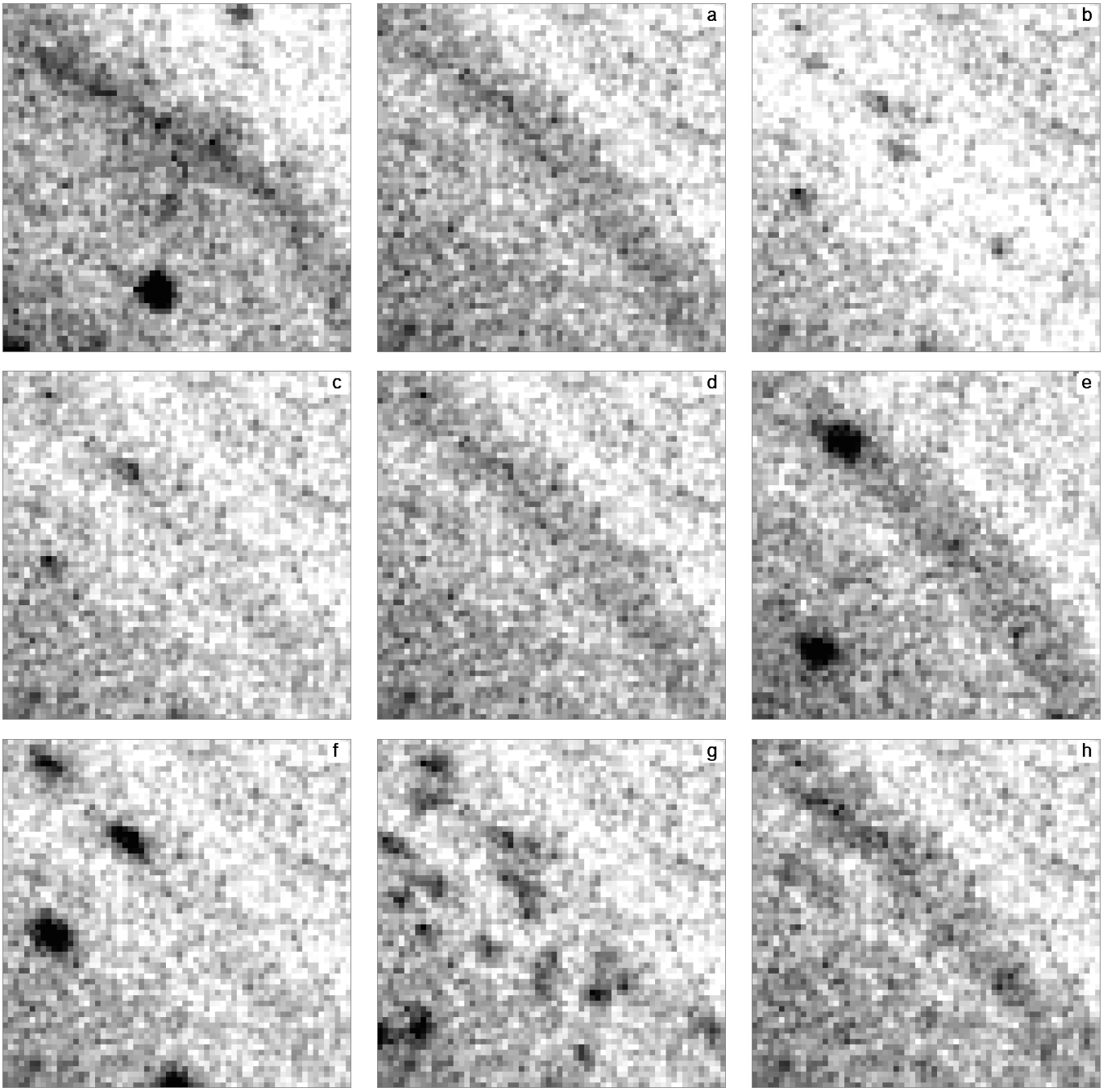

Fig. 6. Close-up image and simulations of the envelope of IRC+10216. *Left to right, top to bottom:* observed image, and simulations **a)–h)** in sequence. See Table 3 for details. The fields are $12\farcs8 \times 12\farcs8$ with $0\farcs2$ pixels.

observations, with simulation h being close to a limiting case. The bottom line of the analysis is that the envelope of IRC+10216 is relatively smooth and probably does not include high density contrast proto-globules.

6. Discussion

6.1. Proto-globules in circumstellar envelopes?

The above results provide good evidence against the presence of high density contrast proto-globules with masses $\gtrsim 1 \times 10^{-5}$ $M_{\odot}$ in the neutral circumstellar envelopes of NGC 7027 and IRC+10216. We believe that these objects are among the most likely precursors of evolved PNe with massive molecular envelopes and neutral globules like the Helix nebula, so unless globules require special conditions not found in NGC 7027 and IRC+10216, our results argue against globule formation in high density contrast instabilities in the atmosphere of the star.

It has been pointed out to us by Dyson (2002) that the globule formation model of Dyson et al. (1989) suggested that the Helix proto-globules might be identified with SiO maser spots

Table 3. Simulations of IRC+10216.

Model	$M_{\rm pg}$ ($M_\odot$)	$N_{\rm pg}$	$\rho_{\rm pg}/\rho_{\rm env}$	$\rho_{\rm pg}/\rho_{\rm sh}$	f	Comments
a	...	0	...	...	0	smooth shell at 34″, no globules
b	3.0×10^{-5}	130	6927	∞	1.0	standard globules
c	3.0×10^{-5}	65	6927	5495	0.5	standard globules
d	3.0×10^{-5}	13	6927	3053	0.1	standard globules
e	3.0×10^{-5}	130	2052[a]	813[a]	0	smooth shell at 34″, plus standard globules at 51″
f	3.0×10^{-5}	65	865	686	0.5	$r_{\rm pg} = 2\,r_{\rm st}$
g	3.0×10^{-6}	650	693	549	0.5	$M_{\rm pg} = M_{\rm st}/10$
h	3.0×10^{-7}	6500	69	55	0.5	$M_{\rm pg} = M_{\rm st}/100$

[a] Density relative to envelope/shell at 34″.

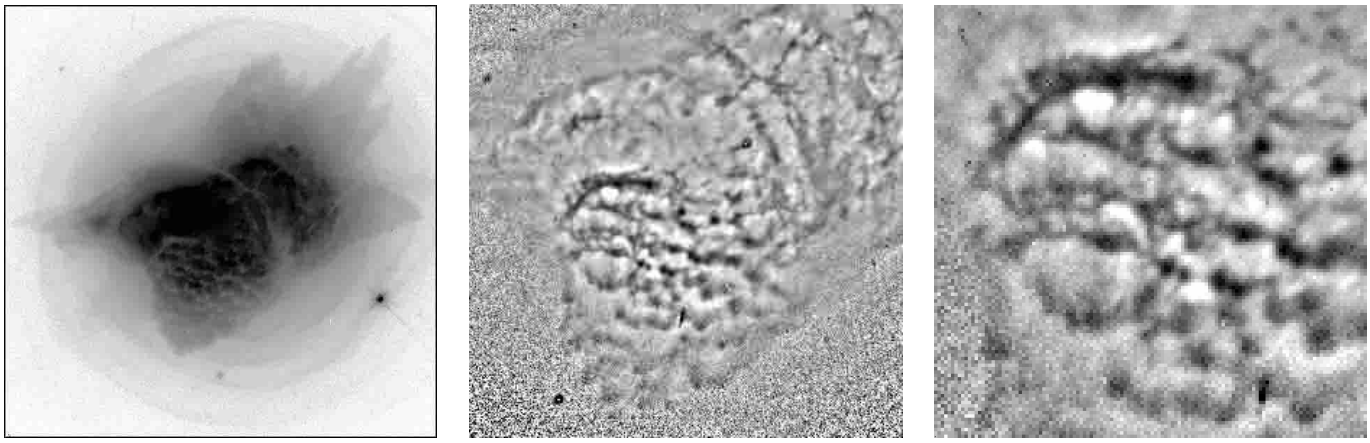

Fig. 7. Structure of the inner circumstellar envelope of NGC 7027: HST WFPC2 images. *Left:* wide-V ($F555W$), field 28.″4 × 28.″4. *Center:* unsharp mask of $I(F555W)/I(814W)$, field 13.″8 × 13.″8. *Right:* close-up of center panel, field 5.″9 × 5.″9. In the left panel, the greyscale is negative (absorption features are light); in the center and right panels, low values of $I(F555W)/I(814W)$, which correspond to absorption features, are dark. The images have been stretched to show details.

in the progenitor AGB envelope, which would imply an O-rich atmosphere, whereas both NGC 7027 and IRC+10216 are C-rich. In fact, the C/O ratio of the Helix nebula is an open question: for the ionized gas, Henry et al. (1999) have measured values of 0.98 and 0.75 at two positions in the nebula, but the uncertainties are too large (∼100%) to draw a definite conclusion on whether it is C- or O-rich. It is clear from HST images, however, that globules very similar to those in the Helix are present in C-rich PNe, e.g., NGC 6720, so the C/O ratio does not appear to be the most important consideration. On the other hand, there could be different paths to globule formation in C- and O-rich envelopes, and this warrants further study.

The relative smoothness of the extended envelopes that we find is perhaps surprising in view of the fact that the inner regions of AGB envelopes close to the central stars are reported to be far from homogeneous (e.g., Tuthill et al. 2000; Osterbart et al. 2000; Kemball & Diamond 1997). Theoretical considerations, however, suggest that initial irregularities can be smoothed out on the smallest size scales as the gas moves away from the star. When the wind velocity exceeds the local sound speed, regions of higher density can be expected to become smooth on size scales $l \lesssim 2c_{\rm o}r/V$ (Sect. 3, see also Morris 1993), and the corresponding angular size scale subtended at the star is $\theta \sim 2c_{\rm o}/V$. This will be largest in the acceleration region, and for representative conditions in IRC+10126 ($T \sim 600$ K at $d \sim 5 \times 10^{14}$ cm, e.g., Keady & Ridgway 1993), $\theta \sim 0.2$ rd or $\sim 10°$. If the bulk motion of the gas in this region is directed radially, rather than in coherent clumps, this angular size scale will be frozen into the flow, and will also characterize the structure farther out.

This description of the evolution of the azimuthal structure in the envelopes is consistent with the observational results given in Sects. 4.1 and 5.1, where the main azimuthal structure is ≳0.1 rd as seen from the central star. The general coherence of the multiple shells seen in IRC+10216 and NGC 7027 also supports this general picture.

6.2. How do globules form?

The absence of proto-globules in the extended envelopes described here is consistent with theoretical models in which globules are formed as the result of instabilities at or near the ionization front of the nebulae as originally proposed by Capriotti (1973); see Dwarkadas (2000) for a summary of more recent work. These models typically assume that the instability develops from an initially homogeneous, spherically

symmetric or axi-symmetric envelope (and, if present, an isotropic, fast stellar wind), so that the properties of the globules (e.g., the mass scale) are the result of the nature of the instability or the global properties of the nebula/envelope.

There are, however, other structural properties of the environment in which PNe form that we propose may also play a role in globule formation: multiple shells, and the shaping effects on the neutral circumstellar gas by directed outflows that occur at the onset of PN formation.

6.2.1. Multiple shells

Multiple shells are present in both the archetypes discussed in this paper, and are therefore likely to be common structures in AGB envelopes. Our analysis of IRC+10216 (Mauron & Huggins 1999, 2000) has shown that the shells are geometrically thin with moderate to high (factors 2–10) shell/inter-shell density contrast. The presence of such structures likely has effects on the propagation of any wind-swept shell and ionization front during the development of the nebula. As they encounter and pass through these structures they will decelerate and then accelerate, and this can be expected to significantly increase the likelihood of instabilities. This also likely affects the impact of more narrowly confined outflows or jets on the circumstellar envelope and could play a role in the specific scenario described below. Detailed models would be of considerable interest.

6.2.2. The transition phase

Major effects take place at or near the onset of PN formation that produce radical changes in the geometrical structure of the neutral circumstellar gas, and are likely to generate microstructure as well. These include a sudden transition to bipolarity which can lead to the formation of equatorial rings, and the action of directed outflows or jets, which are common (e.g., Sahai & Trauger 1998), and are known to produce major shaping of the neutral gas (e.g., Huggins et al. 2000). The jets may induce instabilities in the cavities they create, and if they are multiple in character or precess, they can inscribe the envelope with connected, fragmented structures.

For the objects studied here, IRC+10216 is still on the AGB. Its envelope is roughly spherically symmetric, but it becomes bipolar within a few arc seconds of the star (Fig. 3 of Mauron & Huggins 2000), which corresponds to a recent, sudden ($\lesssim$80 yr) change that may signal the onset of the PN transition. NGC 7027 is more evolved, and the envelope shows a complex, inner structure, which is illustrated in Fig. 7, based on HST WFPC2 images u2sa4501t ($F814W$, 400 s) and u2sa4503t ($F555W$, 200 s), (Bond et al. 1997; Ciardullo et al. 1999; see also Latter et al. 2000).

The features shown in Fig. 7 lie outside the ionized nebula but inside the shells discussed earlier in this paper, their location indicating a relatively recent ($\lesssim$2000 yr) origin in the transition phase. In striking contrast to the smooth shells, these features include numerous micro-jets seen in profile protruding from the inner regions (some are also seen in the close-up image in Fig. 4); a narrow, fragmented equatorial ring and related filaments; and a remarkable, corrugated structure seen in absorption over the face of the nebula. The middle panel of Fig. 7 shows that the corrugations are the result of the micro-jets where they are viewed more face-on along the line of sight. The close-up images of the corrugations show them to be fragmented and linearly connected, stacked parallel to one another.

The micro-jets, which appear to be produced by numerous bullets driven into the neutral envelope, are clearly related to the series of outflows that have created bipolar holes in the neutral circumstellar envelope as discussed by Cox et al. (2002); see also Latter et al. (2000). One possibility is that the outflows actually consist of micro-jets, in which case the layered structure seen in Fig. 7 might result from the precession of the jets. A second possibility is that the micro-jets are secondary structures, caused by the bursting through of material at instabilities in the walls of the cavities made by the primary outflows; this effect has been modeled in the spherically symmetric case for YSOs by Stone et al. (1995), but it could also apply to the directed flows in PNe as well. In either case the result is a highly fragmented inner circumstellar envelope.

Based on the variation in brightness of the corrugations seen in Fig. 7, the opacity of the fragments is $\sim$1 mag. The characteristic width is $\sim$0.″2 which subtends an angle of $\sim$1°–2° at the central star; the thickness of the equatorial ring is similar. These properties are remarkably similar to those we discussed earlier for proto-globules. We believe that the subsequent development of these structures in NGC 7027 can lead to an evolved PN with Helix-like globules. The number of current fragments is probably $\sim$a few hundred, but this could grow by further propagation of the micro-jets, the fragmentation of the filaments, and possibly by the effects of shadowing. The later development of globules with tails is discussed by Huggins et al. (2002).

It is interesting to note that the distribution and kinematics of the neutral gas in the Helix nebula, which includes the individually identified globules and those further out where they merge, shows symmetries which indicate an earlier phase of shaping of the envelope by bipolar outflows (Young et al. 1999). Also, O'Dell et al. (2002) have recently imaged several, nearby, evolved PNe with HST, in addition to the Helix, and suggest that globules may have evolved from linear structures. Both findings support our proposal, illustrated by NGC 7027, that globules develop from the structures created in the neutral envelope at the onset of PN formation.

7. Conclusions

Our analysis of the archetypes IRC+10216 and NGC 7027 provides no evidence for the presence of proto-globules in their extended circumstellar envelopes. The results are consistent with the smoothing out of small scale structure in the wind flow, and argue against the hypothesis that globules in PNe originate in high density contrast clumps formed in the atmosphere of the progenitor AGB star.

We suggest an alternative scenario for the origin of globules in which the neutral circumstellar gas is fragmented at the transition phase by directed outflows or jets.

Acknowledgements. We thank Dr. J. E. Dyson for helpful comments, and Dr. P. de Laverny for providing the VLT image of IRC +10216. The HST data were obtained from the ESA/ESO ST-ECF Archive Center at Garching. This work was supported in part by the CNRS program *Physico-chimie du Milieu Interstellaire* (N.M.), and by NSF grant AST99-86159 (P.J.H.).

References

Atherton, P. D., Hicks, T. R., Robinson, G. J., et al. 1979, ApJ, 232, 786
Bond, H. E. 2000, in Asymmetrical Planetary Nebulae II: From Origins to Microstructures, ed. J. H. Kastner, N. Soker, & S. Rappaport, ASP Conf. Ser., 199, 115
Bond, H. E., Fullton, L. K., Schaefer, K. G., Ciardullo, R., & Sipior, M. 1997, in Planetary Nebulae, ed. H. J. Habing, & H. J. G. L. M. Lamers (Dordrecht: Kluwer), 211
Capriotti, E. R. 1973, ApJ, 179, 495
Ciardullo, R., Bond, H. E., Sipior, M. S., et al. 1999, AJ, 118, 488
Cox, P., Huggins, P. J., Maillard, J.-P., et al. 2002, A&A, 384, 603
de Laverny, P. 2002, in Mass-losing Pulsating Stars and Their Circumstellar Matter, ed. Y. Nakada, & H. Honma (Dordrecht: Kluwer), in press
Dyson, J. E. 2002, private communication
Dyson, J. E., Hartquist, T. W., Pettini, M., & Smith, L. J. 1989, MNRAS, 241, 625
Dwarkadas, V. 2000, in Asymmetrical Planetary Nebulae II: From Origins to Microstructures, ed. J. H. Kastner, N. Soker, & S. Rappaport, ASP Conf. Ser., 199, 379
Hartquist, T. W., & Dyson, J. E. 1997, A&A, 319, 589
Henry, R. B. C., Kwitter, K. B., & Dufour, R. J. 1999, ApJ, 517, 782
Huggins, P. J., Olofsson, H., & Johansson, L. E. B. 1988, ApJ, 332, 1009
Huggins, P. J., Bachiller, R., Cox, P., & Forveille, T. 1992, ApJ, 401, L43
Huggins, P. J., Bachiller, R., Cox, P., & Forveille, T. 1996, A&A, 315, 284
Huggins, P. J., Forveille, T., Bachiller, R., & Cox, P. 2000, ApJ, 544, 889
Huggins, P. J., Forveille, T., Bachiller, R., et al. 2002, ApJ, 573, L55
Jaminet, P. A., Danchi, W. C., Sutton, E. C., et al. 1991, ApJ, 380, 461
Keady, J. J., & Ridgway, S. T. 1993, ApJ, 406, 199
Kemball, A. J., & Diamond, P. J. 1997, ApJ, 481, L111
Kwok, S., Su, K. Y. L., & Stoesz, J. A. 2001, in Post-AGB Objects as a Phase of Stellar Evolution, ed. R. Szczerba, & S. K. Gorny (Dordrecht: Kluwer), 155
Latter, W. B., Dayal, A., Bieging, J. H., et al. 2000, ApJ, 539, 783
Loup, C., Forveille, T., Omont, A., & Paul, J. F. 1993, A&AS, 99, 291
Masson, C. 1989, ApJ, 336, 294
Mauron, N., & Huggins, P. J. 1999, A&A, 349, 203
Mauron, N., & Huggins, P. J. 2000, A&A, 359, 707
Meaburn, J., Walsh, J. R., Clegg, R. E. S., et al. 1992, MNRAS, 255, 177
Morris, M. 1993, in Mass Loss on the AGB and Beyond, ed. H. E. Schwarz (Garching: ESO), 60
O'Dell, C. R., & Handron, K. D. 1996, AJ, 111, 1630
O'Dell, C. R., Balick, B., Hajian, A. R., Henney, W. J., & Burkert, A. 2002, AJ, 123, 3329
Osterbart, R., Balega, Y. Y., Blocker, T., Menshchikov, A. B., & Weigelt, G. 2000, A&A, 357, 169
Sahai, R., & Trauger, J. T. 1998, AJ, 116, 1357
Stone, J. M., Xu, J., & Mundy, L. G. 1995, Nature, 377, 315
Tuthill, P. G., Monnier, J. D., Danchi, W. C., & Lopez, B. 2000, ApJ, 543, 284
Young, K., Cox, P., Huggins, P. J., Forveille, T., & Bachiller, R. 1999, ApJ, 522, 387
Walsh, J. R., & Clegg, R. E. S. 1994, MNRAS, 268, L41